

See discussions, stats, and author profiles for this publication at: <https://www.researchgate.net/publication/257301467>

Cloning and enzymatic characterization of four thermostable fungal endo-1,4- β -xylanases

ARTICLE *in* APPLIED MICROBIOLOGY AND BIOTECHNOLOGY · OCTOBER 2013

Impact Factor: 3.34 · DOI: 10.1007/s00253-013-5244-8 · Source: PubMed

CITATIONS

3

READS

89

6 AUTHORS, INCLUDING:



[Reginald Storms](#)

Concordia University Montreal

66 PUBLICATIONS 4,077 CITATIONS

[SEE PROFILE](#)

Cloning and enzymatic characterization of four thermostable fungal endo-1,4- β -xylanases

Rebecca Sydenham · Yun Zheng · Anja Riemens ·
Adrian Tsang · Justin Powłowski · Reginald Storms

Received: 12 April 2013 / Revised: 17 August 2013 / Accepted: 21 August 2013 / Published online: 2 October 2013
© Springer-Verlag Berlin Heidelberg 2013

Abstract Endo-1,4- β -xylanases (EC 3.2.1.8) hydrolyze the 1,4- β -D-xylosidic linkages in xylans, the most abundant hemicellulose in plant cell walls. Xylanase enzymes have numerous industrial applications, including the manufacturing of animal feed, bread, juice and wine, pulp and paper, and biofuels. In this study, two glycosyl hydrolase family 10 members designated *GtXyn10A* and *GtXyn10B* and two glycosyl hydrolase family 11 members, *OpXyn11A* and *CcXyn11C*, were functionally expressed and subjected to biochemical characterization. The K_M , V_{max} , and k_{cat} values of the four xylanases, determined using birchwood xylan, ranged from 0.27 to 1.1 mg/mL, 130 to 980 μ mol/min/mg, and 109 to 344 s^{-1} , respectively, where *OpXyn11A* gave the highest and *GtXyn10B* the lowest values for all three parameters. Substrate specificity studies and analysis of the products released during the degradation of xylo-oligosaccharides and three types of xylan revealed significant differences in catalytic properties, particularly between *OpXyn11A* and the other xylanases and between the family 10 and the family 11 xylanases. Molecular modeling suggests that the unique substrate specificity of *OpXyn11A* can be attributed to the

presence of a serine rather than an asparagine or aspartate residue at the +1 substrate binding site. Additionally, all four xylanases exhibited biochemical characteristics of interest for various commercial applications.

Keywords Xylanase · GH10 · GH11 · Xylan · Hemicellulases · Glycoside hydrolases

Introduction

Xylan, comprising approximately 25 to 30 % of the mass of vascular plants (Gomez et al. 2008), is a linear polymer of β -1,4-linked xylose residues. Xylans can contain 4-*O*-methyl-D-glucuronic acid ([Me]GlcA), arabinofuranose, and acetyl group substituents attached at various positions along the backbone (Biely 1985). The arabinofuranose side chains may be further substituted with ferulic or *p*-coumaric acids, where ferulic acid can cross-link adjacent cell wall polymers (Grabber et al. 2004). The distribution and type of side chains present in xylan varies between vascular plant species and between tissues within a plant. Hardwood xylans possess [Me]GlcA side chains (Jacobs et al. 2001), whereas wheat arabinoxylan has arabinose side chains (Courtin and Delcour 2002). Other xylans, for example softwood and oat xylan, have both [Me]GlcA and arabinose side chains (Jacobs et al. 2001).

Although recent studies have increased our understanding of xylan structure, further studies are needed to fully elucidate their complex and variable structures (Grabber et al. 2004; Beg et al. 2001). Not surprisingly, important features about xylan structures continue to be discovered. For example, Jacobs et al. (2001) reported that the distribution of [Me]GlcA substituents along the backbone of spruce is periodic, whereas in birch and aspen xylan, the distribution of [Me]GlcA residues is irregular. Bromley et al. (2013) found

R. Sydenham · A. Tsang · R. Storms
Department of Biology, Concordia University, 7141 Sherbrooke
Street West, Montreal, QC H4B 1R6, Canada

Y. Zheng · A. Tsang · J. Powłowski · R. Storms (✉)
Centre for Structural and Functional Genomics, Concordia
University, 7141 Sherbrooke Street West, Montreal, QC H4B 1R6,
Canada
e-mail: storms@alcor.concordia.ca

A. Riemens
DSM Biotechnology Center, Beijerinck Laboratory, PO Box 1,
2600MA, Delft, The Netherlands

J. Powłowski
Department of Chemistry and Biochemistry, Concordia University,
7141 Sherbrooke Street West, Montreal, QC H4B 1R6, Canada

two differentially [Me]GlcA decorated domains in the xylan of *Arabidopsis*. One domain had [Me]GlcA substituents at intervals of eight or ten backbone residues, while the [Me]GlcA residues in the other domain were separated by five, six, or seven residues along the backbone. In another study, Peña et al. (2007) reported that the unique glycosyl sequence 4- β -D-Xylp-(1-4)- β -D-Xylp-(1-3)- α -L-Rhap-(1-2)- α -D-GalpA-(1-4)-D-Xylp is present at the reducing end of xylan backbones from both woody and herbaceous plants.

Given the complex structure of xylooligosaccharides and natural xylans with O₂- and/or O₃-linked arabinofuranose and/or α 1,2-linked [Me]GlcA substituents differed significantly between the GH10 and GH11 members and between *OpXyn11A* and *CcXyn11C*. We also showed that xylan substituents differentially inhibited degradation by the GH10 and GH11 xylanases. Some of these differences apparently arise because the substituent accommodating pockets of the two GH10 xylanases are closer to the catalytic residues than those pockets in the two GH11 xylanases. A major difference observed between *OpXyn11A* and the other xylanases was its inability to hydrolyze xylooligosaccharides shorter than xylopentaose.

Two xylanases, a GH10 and a GH11, have been shown to utilize xylan's side chains to facilitate binding of the substrate (Vardakou et al. 2005, 2008). Residues along the substrate-binding clefts of these enzymes have been found to interact with arabinose residues on the glycone moiety upstream of the newly formed reducing end. The side chain binding site is apparently closer to the catalytic residues in the family 10 xylanase.

Xylanases have numerous industrial applications (Collins et al. 2005), including as an animal feed additive to improve digestibility (Cowieson et al. 2006), in bread-making to help dough rise (Courtin and Delcour 2002), in the clarification of juice and wine (Beg et al. 2001), in pre-bleaching of pulp in the production of paper (Bajpai 2004), in the synthesis of xylitol (Granström et al. 2007) and ethanol from xylan (Polizeli et al. 2005), and for the hydrolysis of biomass for biorefinery applications (Polizeli et al. 2005; Collins et al. 2005; Paës et al. 2012). The use of xylanases for these purposes is more environmentally friendly, and often more cost effective, than chemical alternatives (Subramanyan and Prema 2002); however, few if any of the almost 250 characterized xylanases (Collins et al. 2005; Paës et al. 2012) possess catalytic and physical properties tailored to

meet the specific requirements associated with any of these commercial applications.

In this study, we characterized four novel xylanases, *GtXyn10A* and *GtXyn10B* from *Gloeophyllum trabeum*, *OpXyn11A* from *Ophiostoma piliferum*, and *CcXyn11C* from *Coprinopsis cinerea*. The ability of the xylanases to hydrolyze short xylooligosaccharides and natural xylans with O₂- and/or O₃-linked arabinofuranose and/or α 1,2-linked [Me]GlcA substituents differed significantly between the GH10 and GH11 members and between *OpXyn11A* and *CcXyn11C*. We also showed that xylan substituents differentially inhibited degradation by the GH10 and GH11 xylanases. Some of these differences apparently arise because the substituent accommodating pockets of the two GH10 xylanases are closer to the catalytic residues than those pockets in the two GH11 xylanases. A major difference observed between *OpXyn11A* and the other xylanases was its inability to hydrolyze xylooligosaccharides shorter than xylopentaose.

Materials and methods

Preparation of the mycelial masses used for RNA isolation

Primary cultures were prepared by inoculating 200 mL of media, yeast malt broth (YM) (Atlas and Park 1993) for *O. piliferum*, and mycological broth (Huppert and Walker 1958) supplemented with 1 mL of trace element solution (Mandels et al. 1976) for *C. cinerea* and *G. trabeum*. The primary cultures were inoculated with several 1-cm diameter plugs taken from 1.5 % agar plates prepared using the same media formulations. The cultures were shaken at 150 to 200 rpm with a marble at the optimal temperature for each strain (*G. trabeum* 25 °C, *O. piliferum* 25 °C, and *C. cinerea* 37 °C) until sufficient mycelia (2 to 5 g wet weight) accumulated. Mycelial masses were harvested on Buchner funnels fitted with sterile miracloth filters, washed with two volumes of sterile distilled water and suspended in 200 ml of sterile distilled water. The suspended mycelia were used to inoculate cultures for producing mycelial masses for RNA extraction.

Mycelial masses for RNA extraction were prepared using at least 13 of the following culture media. The culture media used were YM, *Trametes*-defined medium (TDM) (Reid and Paice 1994), and 21 versions of TDM medium modified as follows: (1) asparagine (0.75 g L⁻¹), (2) MnSO₄ omitted from the trace elements, (3) 0.2 mM MnSO₄, (4) 20 μ M CuSO₄, (5) 10 g L⁻¹ cellulose (Solka-Floc 200 FCC, Sigma, St. Louis, MO, USA) as the sole carbon source, (6) 10 g L⁻¹ birchwood xylan as the sole carbon source, (7) 10 g L⁻¹ food grade wheat bran as the sole carbon source, (8) 10 g L⁻¹ citrus pectin as the sole carbon source, (9) Tween 80 omitted, (10) 5.0 g L⁻¹ ground hardwood Kraft Pulp as the sole carbon source, (11) initial culture pH 7.5, (12) KH₂PO₄ replaced by 5 mM phytic

acid (Sigma), (13) 10 g L⁻¹ olive oil (Sigma) as the sole carbon source, (14) glucose omitted and half the distilled water replaced by whitewater waste produced during the manufacturing of peroxide bleached pulp, (15) 10 g L⁻¹ tallow as the sole carbon source, (16) 10 g L⁻¹ defined lipid (Sigma) as the sole carbon source, (17) 10 g L⁻¹ xylose as the sole carbon source, (18) glucose omitted and half the distilled water replaced with a 1:1 ratio of whitewater waste produced during the manufacturing of newsprint and peroxide bleached pulp, (19) initial culture pH 8.5, (20) 5 g L⁻¹ yellow grease as the sole carbon source, and (21) initial pH of 8.84. All cultures were prepared by inoculating 5 ml of the suspended mycelial mass from the primary cultures into 500-mL Erlenmeyer flasks containing 95 ml of the various media and a marble. The cultures were incubated at 150 to 200 rpm at the optimal growth temperature for each strain until 1 to 2 g wet weight of mycelia was produced.

Mycelia masses were harvested as described above and stored at -80 °C. *G. trabeum* mycelia were isolated using all of the above media except modified TDM versions 12, 13, 14, 15, 16, 17, 19, 20, and 21. *O. piliferum* mycelia were isolated using all of the above media except YM medium and modified TDM versions 11, 16, 17, 18, and 19. *C. cinerea* mycelia were isolated using all of the above media except YM and the modified TDM versions 3, 10, 12, 13, 14, 15, 17, 20, and 21. *G. trabeum* and *O. piliferum* mycelia were also isolated using from TDM cultures incubated at 5 °C above their optimal temperatures.

Enzyme selection process

cDNA libraries were constructed and EST tags generated as described by Semova et al. (2006). The EST sequences, available at <https://fungalgenomics.concordia.ca/feadb/download.php>, were searched to identify full length cDNA clones encoding xylanases in three steps. First, the OrfPredictor web server (Min et al. 2005a) was used to identify full-length cDNAs using EST sequences. Next, full-length cDNAs encoding putative xylanases were identified by searching the full-length cDNAs using the web server TargetIdentifier (Min et al. 2005b), which uses BLASTX alignments to locate protein coding regions and assign putative functions in query sequences. Finally, xylanases encoding full-length cDNAs identified in steps one and two were manually annotated. Two of these were found in *G. trabeum* (American Type Culture Collection, strain ATCC #11539), one in *O. piliferum* (Forintek culture collection, strain FCC # 55A), and the last in *C. cinerea* (Fungal Genetics Stock Centre, strain FGSC #9003 alternate designation Okayama 7 [#130]). One full-length cDNA for each xylanase was fully sequenced on both strands. After PCR-amplification using high-fidelity thermostable polymerases, the open reading frames (ORFs) were transferred into the Gateway compatible

entry vector pDONR201 (Invitrogen, Life Technologies, Grand Island, NY, USA) by in vitro recombination. Finally, the xylanase ORFs were transferred by in vitro recombination from the entry clones into pGBFIN-GTW (Tambor et al. 2012), a Gateway compatible expression vector derived from pGBFIN (van den Brink et al. 1999). The resulting pGBFIN-GTW clones were transformed into *Aspergillus niger* strain CBS 513.88 (FGSC A1513).

Filtered media from cultures of the subsequent *A. niger* transformants were examined by SDS-PAGE and xylanase assays to assess xylanase expression. The sequences of the cDNAs encoding the four xylanases have been deposited in GenBank; the accession numbers are JN971032 (*xyn10A*), JN971033 (*xyn10B*), JN971034 (*xyn11A*), and JN971035 (*xyn11C*).

Bioinformatic analysis

Amino acid sequence alignments were generated using ClustalIX (Larkin et al. 2007). Catalytic residues were identified based on these alignments, which included families 10 and 11 xylanases that had their catalytic residues identified through site-directed mutagenesis and biochemical analyses (Moreau et al. 1994; Wakarchuk et al. 1994). Conserved domains were identified using a combination of the NCBI Conserved Domain Database and Search Service v2.14 (Marchler-Bauer and Bryant 2004), ScanProsite (de Castro et al. 2006), InterProScan (Quevillon et al. 2005), and the Motif Scan tool on the MyHits website of the Swiss Institute of Bioinformatics (Pagni et al. 2007). The SignalP 3.0 server (Bendtsen et al. 2004) was used to identify signal peptides.

3D models were generated by SWISS-MODEL Workspace (Arnold et al. 2006; Schwede et al. 2003) using template structures from the SWISS-MODEL Repository (Kopp and Schwede 2004). The templates used for the catalytic domains and CBM were PDB IDs 1I1WA, 3CUIA, 1CBHA, 1TE1B, and 1XNKA (Natesh et al. 2003; doi:10.2210/pdb2cui/pdb; Kraulis et al. 1989; Payan et al. 2004; Jänis et al. 2005). The templates used for the substrate binding regions were 2BNJ and 2VGD (Vardakou et al. 2005, 2008). Images of the modeled structures were generated using the PyMOL Molecular Graphics System, ver. 1.3r1 edu (Schrödinger, LLC, New York, NY, USA). The quality of each model was assessed using Qmean (Benkert et al. 2008) and Procheck (Laskowski et al. 1993) as well as other assessment tools found on the Protein Structure & Model Assessment Tools page of the SWISS-MODEL Workspace (Arnold et al. 2006).

Enzyme preparation

The cloned xylanases were expressed in *A. niger* strain CBS 513.88. The CBS 513.88 transformants and the empty vector (pGBFIN-GTW) control (VTO) were grown in 100 mL of liquid medium as described previously for 5 days at 34 °C and

170 rpm (Tambor et al. 2012). Culture supernatants were harvested by centrifugation at 5,000 rpm for 20 min followed by filtration through Whatman GF/A filters (GE Healthcare Life Sciences, Piscataway, NJ). Sugars were removed from the filtered samples using centrifugal filter devices (Ultrafree-0.5, Millipore, Billerica, MA, USA), and the samples were buffer exchanged into sodium citrate buffer (10 mM, pH 4.5). A preliminary estimate of xylanase activity in the culture filtrates of the transformants and the empty vector control was performed using the xylanase assay described previously (Decelle et al. 2004). The protein concentration of the xylanases was determined by running 10 µL of appropriately diluted samples on 14 % SDS-PAGE gels and comparing band intensities to 1.0, 0.75, 0.50, and 0.25 µg of BSA standards using GeneTools software (Syngene USA, Frederick, MD).

Xylanase activity assays

pH and temperature optima and thermostability were estimated using azo-xylan (Megazyme, Bray, Ireland) as the substrate following the manufacturer-supplied protocol, except that the reaction volume used was 100 µL and the assay was performed in 96-well microtiter plates. The pH optimum of each enzyme was estimated using the following buffers: 100 mM citric acid-Na₂HPO₄ (pH 3 to 6.5), 100 mM Na₂HPO₄-Na₂HPO₄ (pH 6.5 to 7.5), and 100 mM Tris-HCl (pH 7.5 to 8.7). Temperature optima were estimated by performing the same assay at various temperatures from 20 to 90 °C at the pH optimum of each enzyme. Enzyme thermostability was assessed by pre-incubating at various temperatures from 0 to 90 °C for 1 h, followed by incubation for 15 min with azo-xylan at the pH and temperature optimum of each enzyme.

Enzyme kinetic parameters were estimated using birchwood xylan (Sigma-Aldrich, St. Louis, MO, USA) as the substrate and the bicinchoninic acid (BCA) method adapted for 96-well microplates (Grishutin et al. 2004) to detect reducing sugar products. Enzyme activity assays were performed in triplicate using various concentrations (0.3–3.9 mg/mL) of birchwood xylan in 200 µL of 75 mM citric acid-Na₂HPO₄ buffer at the pH optimum of each enzyme and 37 °C. Aliquots of 10 µL were removed from each reaction mixture at 6-min intervals over a time course of 30 min so that initial rates could be established. Reaction mixture aliquots were incubated at 80 °C for 30 min with BCA reagent (100 µL) and distilled water (90 µL), and then the absorbance at 562 nm was measured for 80 µL aliquots. Using a standard curve generated with D-xylose, absorbance was converted into micromoles of reducing sugar ends produced. One unit of enzyme activity is defined as the amount of enzyme that produces 1 µmol of reducing ends per minute. Michaelis–Menten kinetics were observed for each enzyme, and K_M and V_{max} parameters were estimated by nonlinear regression using GraphPad Prism version 5.0 (Motulsky and Brown 2006).

Fig. 1 Amino acid sequence alignments. **a** Alignment of xylanases *GtXyn10A* and *GtXyn10B* with GH10 xylanases XynA from *Thermoascus aurantiacus* [P23360] and Cex from *Cellulomonas fimi* [AAA56792] whose crystal structures were used to generate our 3D models, and XynC and XynA [AAG44993] from *P. chrysosporium*, which have been biochemically characterized. CBM domains are enclosed in a solid box. Grey shaded boxes highlight GH10 motifs, with the active site pattern shown in white letters and vertical arrows indicating active site glutamates. The red letters indicate the residues found in the substrate binding cleft. The brackets enclose the full GH10 conserved domain. The horizontal arrow indicates the linker region between the CBM and the catalytic domain. Two potential N-glycosylation sites (four residues long) are highlighted in black. The four cysteine residues predicted to form disulphide bridges are highlighted in grey. **b** Alignment of the predicted CBM domain of *GtXyn10B* with the CBM domains of CBH1 from *T. reesei* [GI:157830153], and XynC [ABZ88799] and XynA [AAG44993] from *P. chrysosporium*. The four cysteine residues predicted to form disulphide bridges are highlighted in grey, with grey lines indicating how they interact. **c** alignment of xylanases *OpXyn11A* and *CcXyn11C* with GH11 xylanases XynB from *P. chrysosporium* [AAG44995], XynC from *Penicillium funiculosum* [GI:51247634], and XynA from *Thermomyces lanuginosus* [GI:157834320]. GH11 motifs, conserved domains, active site patterns, catalytic glutamate residues, substrate binding residues, and potential N-glycosylation sites are indicated as in **a**

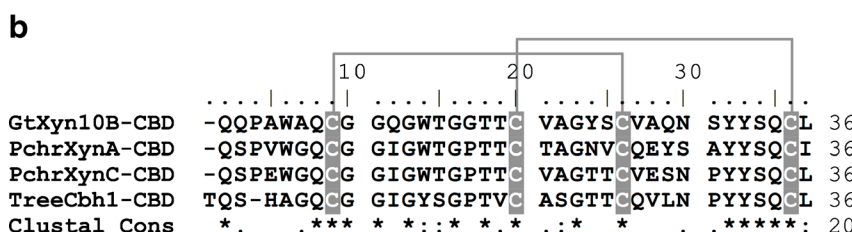
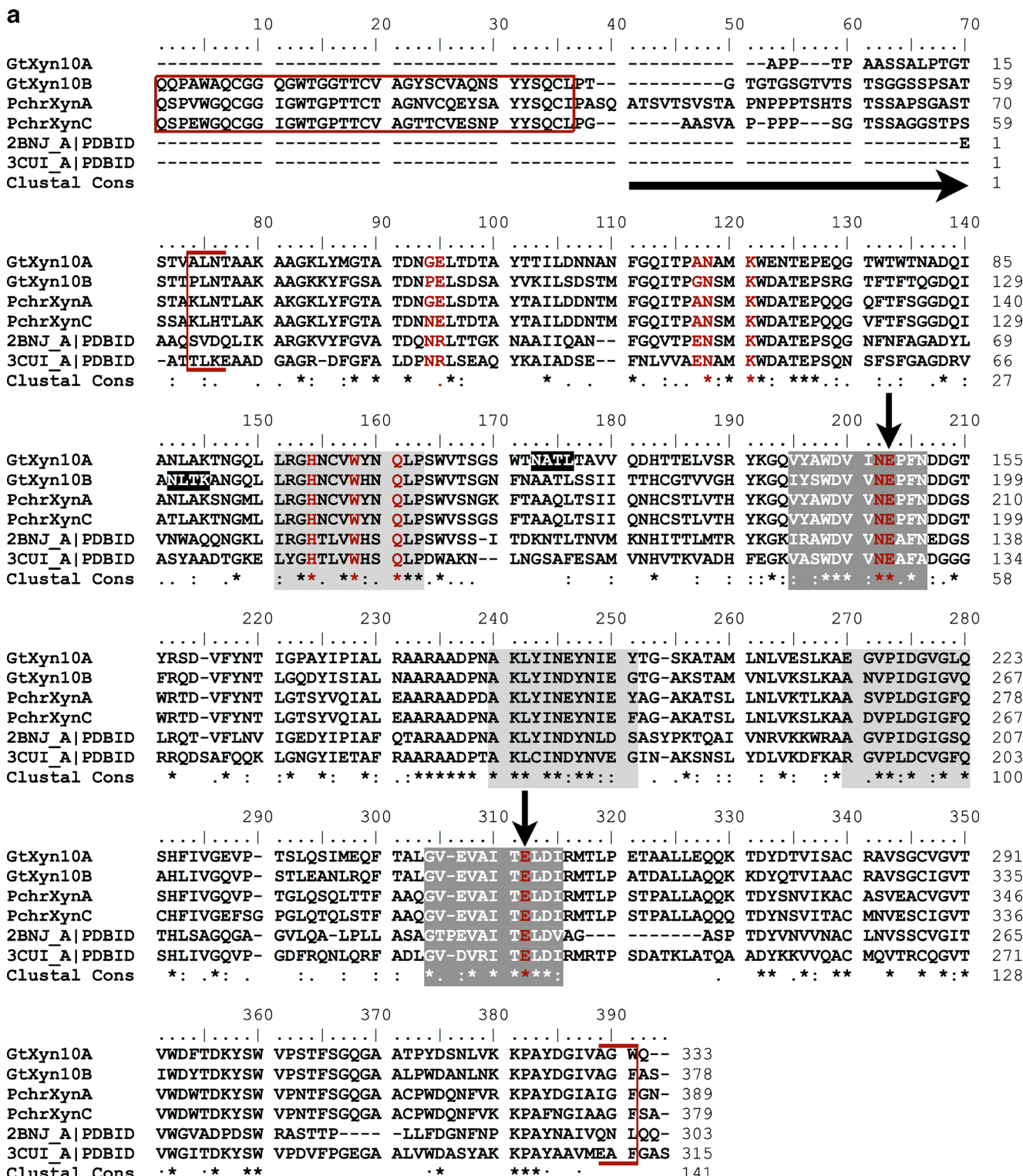
Specific activity and substrate specificity assays were performed at the pH and temperature optima for each enzyme using final concentrations of 5 mg/mL of birchwood xylan (Sigma-Aldrich), beechwood xylan (Sigma-Aldrich), wheat arabinoxylan (Megazyme), sugar beet arabinan (Megazyme), carboxymethyl cellulose 4 M (CMC-4 M; Megazyme), glucomannan, or xyloglucan (Megazyme). Enzyme activity was quantified using the BCA method.

Analysis of hydrolysis products by thin layer chromatography

The hydrolyses of xylo-oligomers (Megazyme), birchwood (Sigma-Aldrich), beechwood (Sigma-Aldrich), and wheat xylan (Megazyme) were carried out in volumes of 80 µL with 5 mg/mL substrate at the pH optimum of each enzyme. Two sets of 24-h reactions were performed for each enzyme: one at 37 °C and the second at its temperature optimum. Thin layer chromatography (TLC) was performed as described previously (Decelle et al. 2004). Reaction products, equivalent to 50 µg of substrate in the initial reaction mixture, were spotted on silica G TLC plates (Analtech, Newark, DE, USA).

Identification of xylan hydrolysis products by mass spectrometry

Reaction products for mass spectrometry were generated as described for TLC analysis, except that 10-mM acetate buffer was used, and samples were diluted 10-fold or 100-fold in cold 50 % (v/v) acetonitrile. Undiluted or diluted samples were then mixed in a 1:1 ratio with 2,5-dihydroxybenzoic acid (Sigma-Aldrich) (10 mg/mL in 30 % (v/v) acetonitrile).



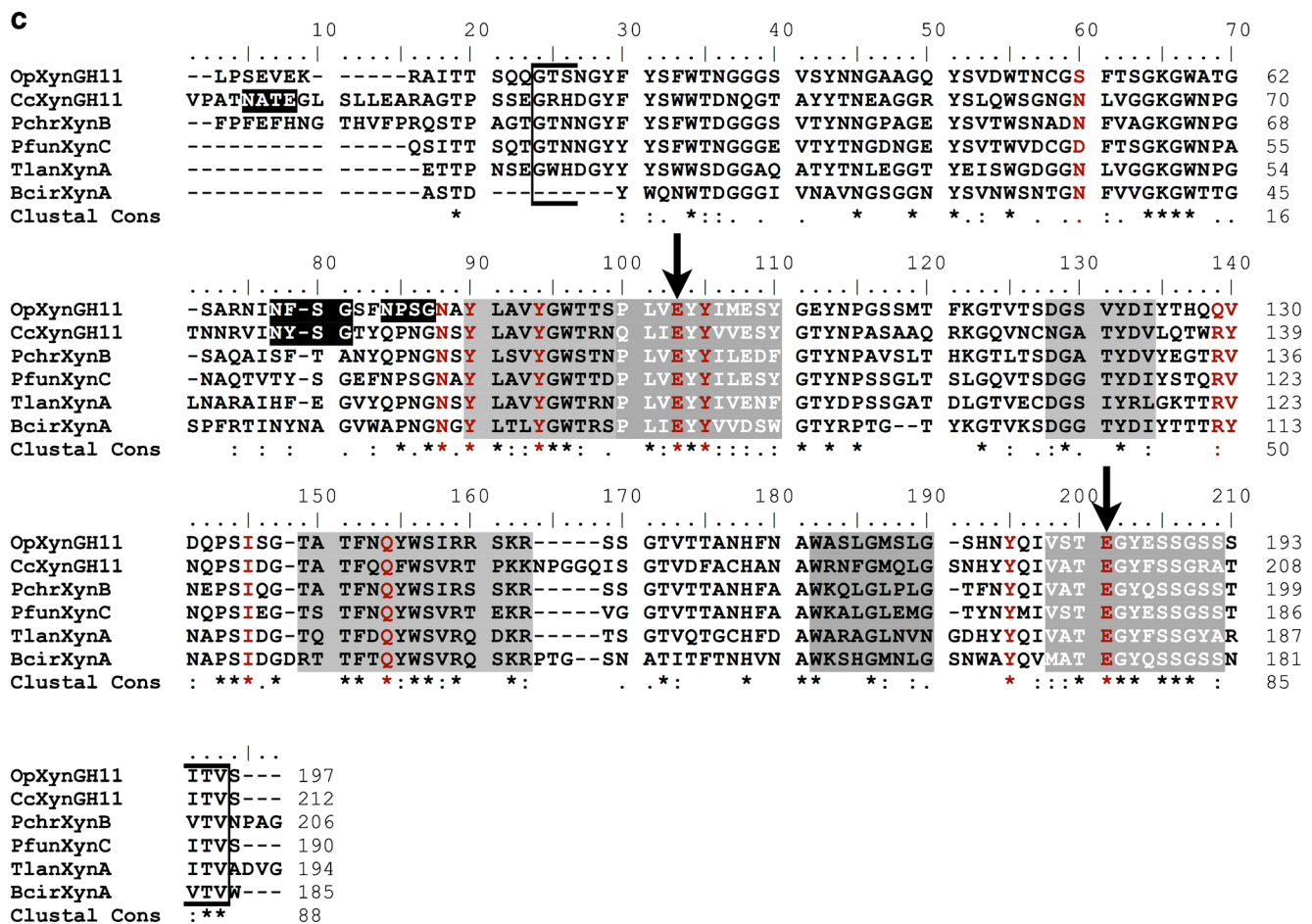


Fig. 1 (continued)

One microliter of the resulting mixture was then spotted on a MALDI plate and masses measured using a Micromass M@LDI™ MALDI-TOF mass spectrometer (Waters, Milford, MA, USA). Masses obtained were compared with previously published mass spectrometry results from xylan hydrolysates (Kabel et al. 2007) and with masses derived using the following formula:

$$\text{MW}_{\text{Na}} + \text{MW}_X + (n_X - 1)\text{MW}_{X-\text{H}_2\text{O}} + n_{[\text{Me}]\text{GlcA}}\text{MW}_{[\text{Me}]\text{GlcA}-\text{H}_2\text{O}} \\ + n_{\text{Ac}}\text{MW}_{\text{Ac}} + n_{\text{CA-Ara}}\text{MW}_{\text{CA-Ara}-\text{H}_2\text{O}} + n_{\text{FA-Ara}}\text{MW}_{\text{FA-Ara}-\text{H}_2\text{O}}$$

Where MW=molecular weight, n=number of particular monomer, Na=sodium, X=xylose, [Me]GlcA=methylated glucuronic acid, Ac=acetyl group, CA=coumaric acid, Ara=arabinose, and FA=ferulic acid.

Results

Sequence analysis and 3D modeling

Four fungal endo-1,4- β -xylanases were cloned, sequenced, and successfully expressed. BLASTP searches at NCBI

revealed similarity between the amino acid sequences of the four xylanases and those of previously characterized xylanases as follows: *GtXyn10A* and *GtXyn10B* shared 71 and 67 % identity with XynA from *Phanerochaete chrysosporium* [AEK97220.1], *OpXyn11A* shared 86 % identity with XYN11F63 from *Penicillium* sp. CGMCC 1669 [ACY70400.1], and *CcXyn11C* shared 73 % identity with XynA from *Schizophyllum commune* [P35809.1]. Conserved domain searches and amino acid sequence alignments of the four xylanases with other GH10 and GH11 xylanases revealed conserved bipartite active site motifs typical of GH10 glycoside hydrolases in both *GtXyn10A* and *GtXyn10B* and active site signatures typical of GH11 hydrolases in *OpXyn11A* and *CcXyn11C* (Fig. 1a, c). The conserved domain search also predicted that *GtXyn10B* possessed a family 1 carbohydrate-binding module, formerly referred to as a type I cellulose-binding domain (Gilkes et al. 1991), linked by a low complexity 27-residue region to the N-terminus of the catalytic domain (Fig. 1a, b). The alignments also revealed that 85 of 308 and 53 of 181 catalytic domain residues were strictly conserved among the six GH10 xylanases (Fig. 1a), and the six GH11 xylanases (Fig. 1c). Signal P predicted that all four xylanases were translated as pre-proteins with signal peptides

of 18 residues for *GtXyn10A*, *GtXyn10B*, *OpXyn11A*, and 19 residues for *CcXyn11C* (data not shown). After signal peptide removal, the predicted molecular masses and pls of *GtXyn10A*, *GtXyn10B*, *OpXyn11A*, and *CcXyn11C* were 36.0, 39.9, 21.0, and 23.4 kDa, and 4.51, 5.72, 5.84, and 8.47, respectively.

Structures of the four xylanases were generated using SWISS-MODEL. The structures in Figs. 2 and 3 were colored according to quality of the fit, with the best being blue and the worst red. The quality assessment is summarized in Table 1. The Qmean values, Z-scores, and Ramachandran plots for each structure fell well within the range of values obtained with 3D structures determined by x-ray crystallography. The modeled structures of both *GtXyn10A* and *GtXyn10B* (Fig. 2) were eightfold β/α -barrel structures typical of GH10 xylanases. As is typical of GH11 xylanase structures (Davies and Henrissat 1995), *OpXyn11A* and *CcXyn11C* were β -jelly rolls (Fig. 3), principally composed of β -sheets. The protein modeling results, which position the active site residues on opposite walls of the substrate binding clefts of the four xylanases, support the active site residue predictions derived from the ClustalX alignments.

Another set of models (Fig. 4) was prepared based on a GH10 xylanase from *Thermoascus aurantiacus* (*TaXyn10*) and an environmentally isolated GH11 xylanase (*EnXyn11A*), which were crystallized along with xylo-oligomers with arabinose and ferulic acid substituents (Vardakou et al. 2005, 2008). The residues that interact with the xylose backbone are highly conserved between the modeled xylanases and the template

structures; however, in the case of *OpXyn11A*, there is one key difference, Ser52 replaces Asn48, which interacts with the same xylose residue as Glu184, the catalytic nucleophile. Although serine is capable of hydrogen bonding, its side chain is one carbon shorter and may, therefore, not be available to interact with the substrate (Fig. 4c).

The only substrate-interacting residues to differ between *GtXyn10A* and *GtXyn10B* and those of *TaXyn10* are three of the four residues that form hydrogen bonds with the arabinose side chain of the xylo-oligosaccharide. Where the *TaXyn10* has four such residues, both *GtXyn10A* and *GtXyn10B* have two residues that are capable of hydrogen bonding and two that are unlikely to form any type of interaction with the substrate. Where *TaXyn10* has an asparagine (Asn25), *GtXyn10A* has glycine, and *GtXyn10B* has a proline. Where *TaXyn10* has a glutamate (Glu46), *GtXyn10A* has an alanine, and *GtXyn10B* has a glycine. There is one further amino acid difference that may promote binding of arabinose by both *GtXyn10A* and *GtXyn10B*, where Asp273 in *TaXyn10* is replaced by tyrosine in both enzymes (Fig. 4).

Xylanase production

A. niger VTO transformants expressed less than 0.06 U of xylanase activity per milliliter of culture filtrate, whereas transformants harboring *GtXyn10A*, *GtXyn10B*, *OpXyn11A*, and *CcXyn11C* expressed 450, 221, 69.5, and 210 U/mL of culture filtrate, respectively. The relative molecular masses of *GtXyn10A*, *GtXyn10B*, *OpXyn11A*, and

Fig. 2 Predicted ribbon structures of the catalytic domains of each GH10 xylanase. **a** *GtXyn10A* and **b** *GtXyn10B*, along with **c** the predicted ribbon structure of the CBD1 domain of *GtXyn10B*. Two different perspectives are shown for each catalytic domain: one looking down into the $(\beta/\alpha)_8$ barrel as well as a view taken at right angles to the $(\beta/\alpha)_8$ barrel. Active site glutamic acid residues are presented in stick format. The structures are colored using a scale from red to blue representing the quality of the fit, with red being the worst and blue being the best. The disulphide bridges of the CBD1 domain are shown in yellow

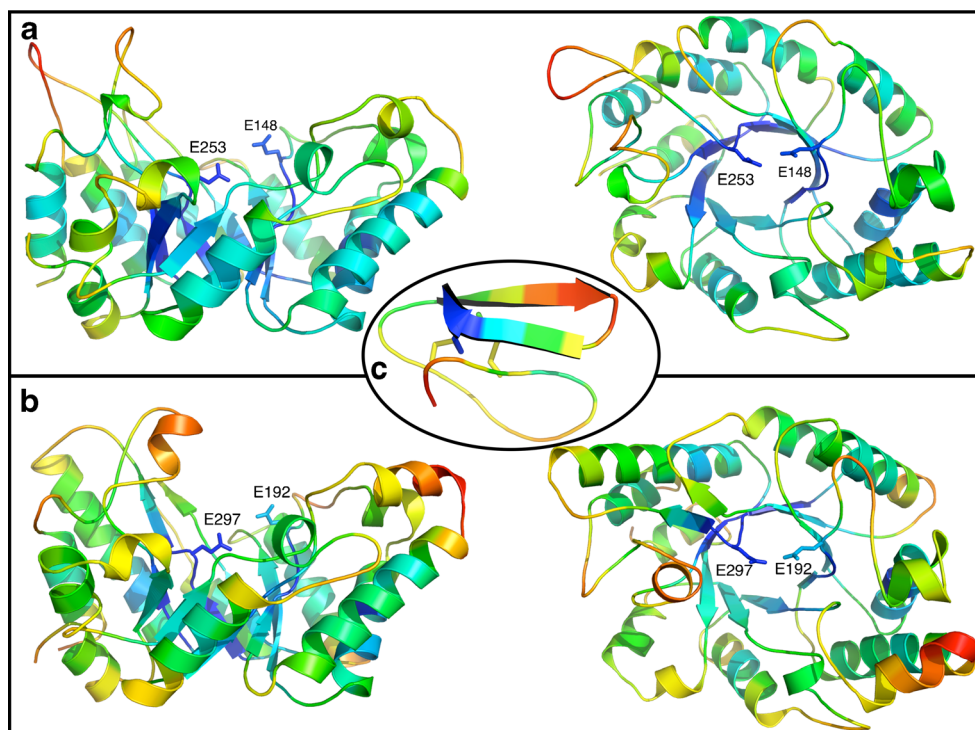
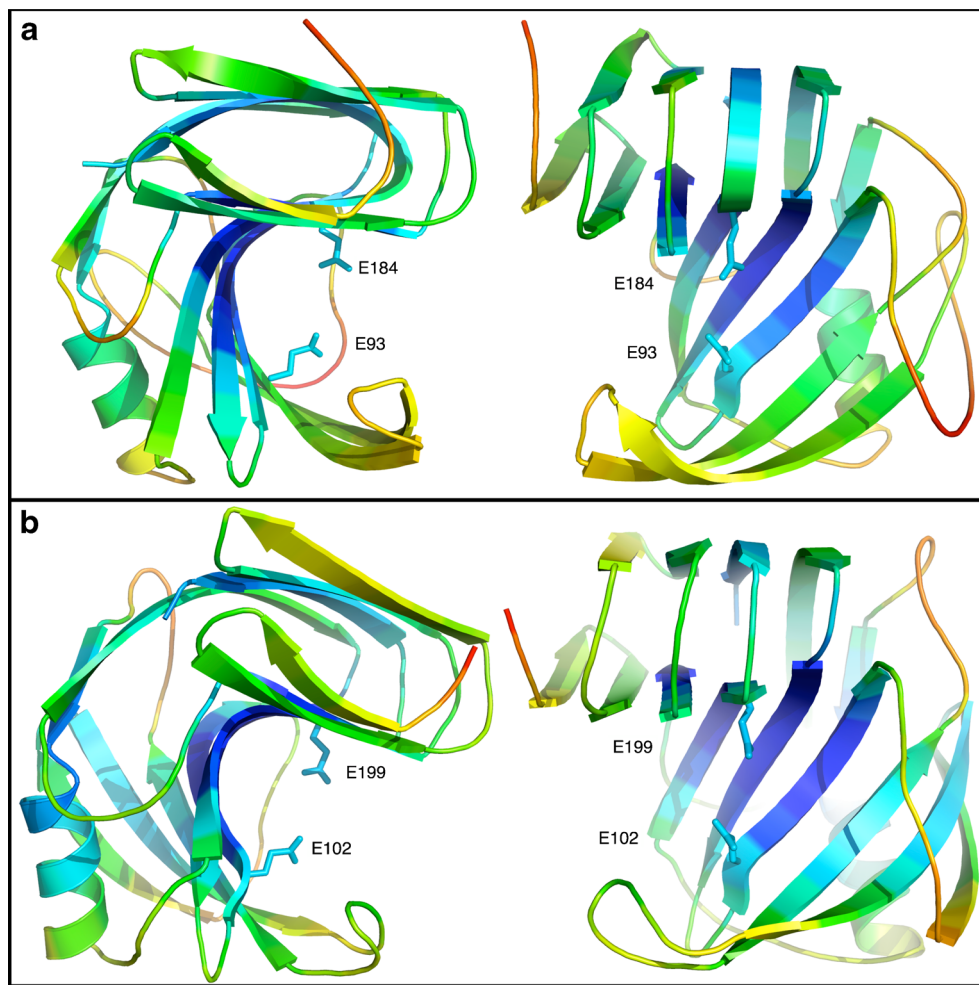


Fig. 3 Predicted 3D β -jelly roll structures of the catalytic domains of each GH11 xylanase. **a** *OpXyn11A* and **b** *CcXyn11C* depicted as described in the legend for Fig. 2



CcXyn11C were 40, 50, 19, and 21 kDa, respectively, as estimated by SDS-PAGE analysis (data not shown). The two GH10 xylanases appeared larger than predicted, which is most likely due to posttranslational modification. In support of this possibility, ScanProsite identified potential N-glycosylation sites in both of the GH10 xylanases (Fig. 1).

Biochemical parameters

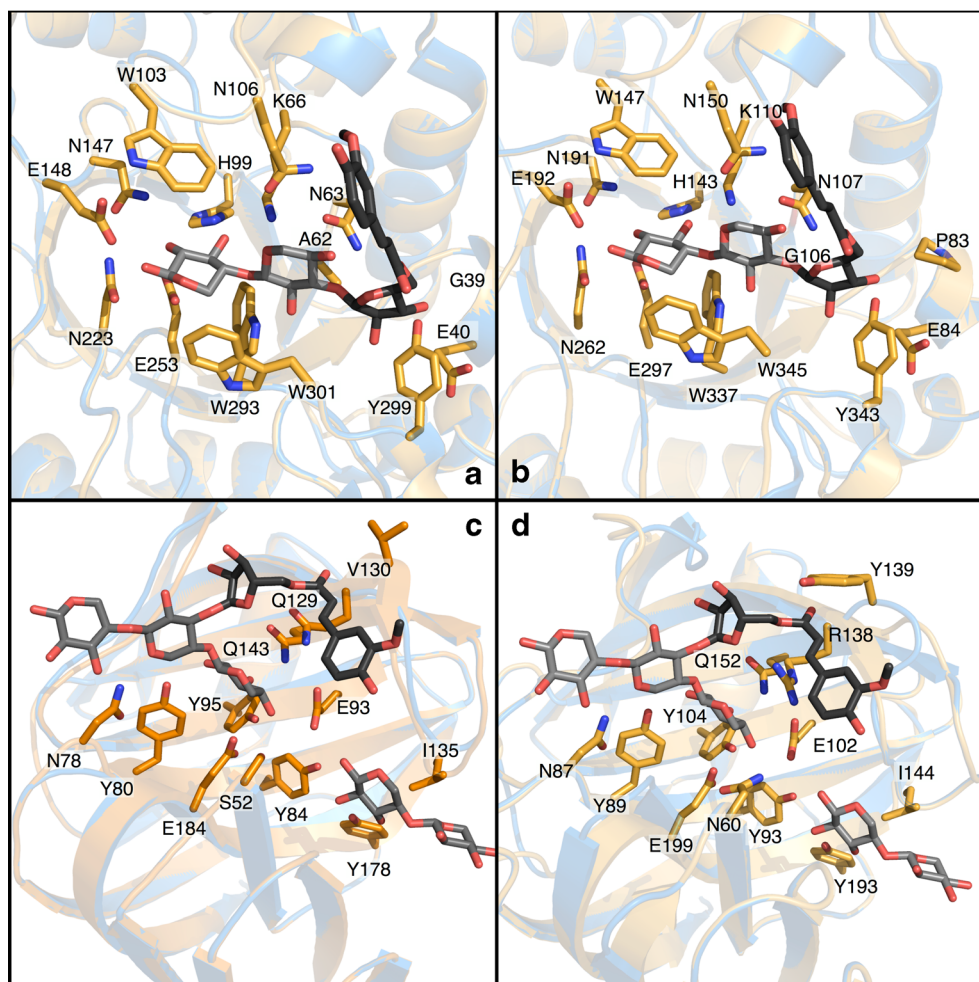
The biochemical properties of the four xylanases were determined. The K_m , V_{max} , and k_{cat} values ranged from 0.27 to 1.1 mg/mL, 130 to 980 $\mu\text{mol}/\text{min}/\text{mg}$, and 109 to 344 s^{-1} , respectively (Table 2). The temperature optima of *GtXyn10A*,

Table 1 Quality assessment of 3D models

	Identity	Q-mean	Z-score	Ramachandran data—with limits			
				Bond length	Bond angle	Planar group	Core
<i>GtXyn10A</i>	45 %	0.737	-0.41	98.8 %	95.9 %	78.4 %	81.8 %
1i1w		0.934	1.86	96.2 %	95.7 %	85.0 %	91.0 %
<i>GtXyn10B</i>	48 %	0.812	0.29	100.0 %	97.4 %	84.8 %	87.7 %
3cuiA		0.911	1.28	100.0 %	99.5 %	100.0 %	89.9 %
<i>OpXyn11A</i>	70 %	0.601	-0.97	100.0 %	98.7 %	85.3 %	75.0 %
1te1B		0.623	-0.82	100.0 %	99.2 %	100.0 %	78.5 %
<i>CcXyn11C</i>	64 %	0.675	-0.34	100.0 %	98.0 %	83.7 %	84.9 %
1xnkA		0.752	1.00	100.0 %	97.3 %	97.4 %	89.8 %
CBD	51 %	0.392	-0.40	100.0 %	98.3 %	90.9 %	73.1 %
1cbhA		0.378	-0.60	93.6 %	99.2 %	100.0 %	73.1 %

Qmean, Qmean Z, and Ramachandran plot scores are shown for the templates used and the derived structures

Fig. 4 Predicted 3D structures of the substrate-binding regions of each xylanase with substituted xylo-oligosaccharides bound. **a** *GtXyn10A*, **b** *GtXyn10B*, **c** *OpXyn11A*, and **d** *CcXyn11C*. All modeled structures are shown superimposed over their templates, with the model in orange and the template in blue. The amino acid side chains participating in binding of the substrate appear in stick format. The xylose backbone of the substrate is shown in light grey, and the arabinose and ferulic acid residues are shown in dark grey. Oxygen molecules within the side chains and substrate are shown in red, and nitrogen molecules are in blue



GtXyn10B, *OpXyn11A*, and *CcXyn11C* were 50, 70, 30–50, and 50–60 °C (Fig. 5a). Neither GH10 xylanase lost

significant activity during preincubation for 1 h at 60 °C; however, they retained less than 2 % activity after 1 h

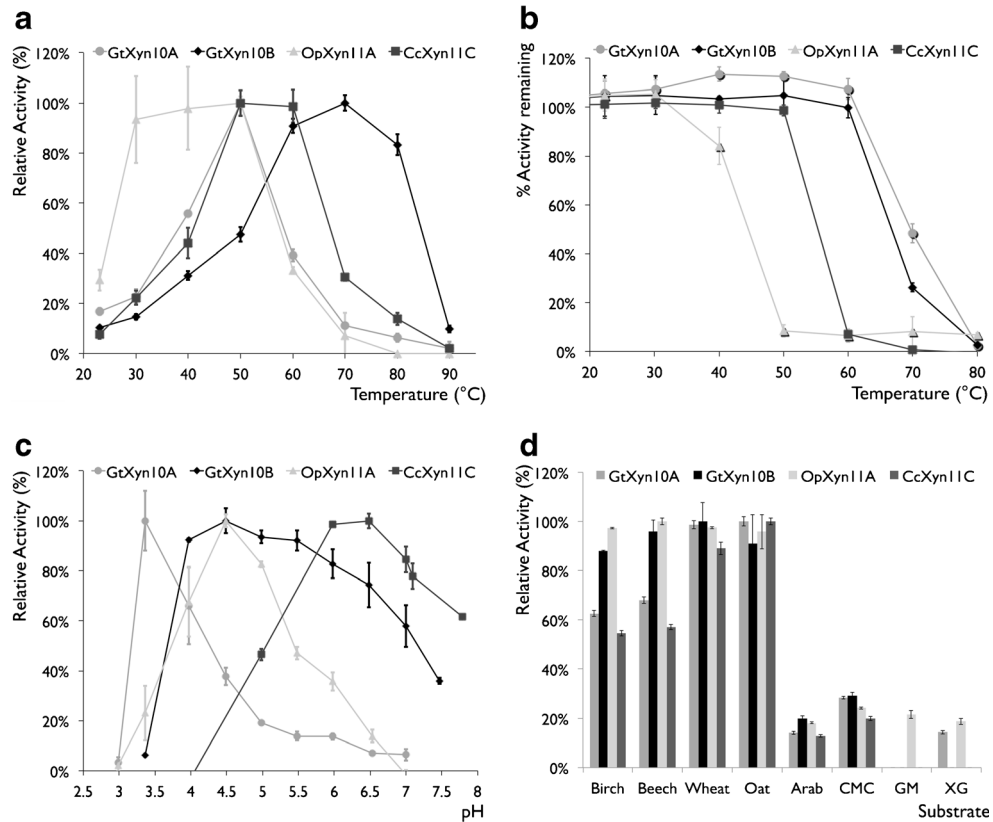
Table 2 Xylanases kinetic and expression data

	V_{max} (μmol/ min/mg)	K_M (mg/mL)	k_{cat} (s ⁻¹)	k_{cat}/K_M	Expression (mg/mL) ^b	SDS-PAGE ^a	
						Xyn	VTO
<i>GtXyn10A</i>	180 ± 4.3	0.40 ± 0.04	109 ± 2.6	272 ± 28	0.88		
<i>GtXyn10B</i>	130 ± 3.3	0.27 ± 0.04	84.5 ± 2.2	395 ± 59	0.34		
<i>OpXyn11A</i>	980 ± 49	1.1 ± 0.2	344 ± 17	290 ± 55	0.053		
<i>CcXyn11C</i>	370 ± 11	0.54 ± 0.06	145 ± 4.3	240 ± 28	0.090		

^a SDS-PAGE analysis of culture filtrates from *A. niger* expressing the four xylanases and the negative control, a culture filtrate from *A. niger* transformed with the expression vector without a cDNA-derived insert (VTO). Each image represents buffer exchanged culture filtrate diluted sufficiently to show xylanase bands of similar intensity. The VTO was desalts and diluted to the same extent as the least diluted sample xylanase (*OpXyn11A*)

^b Secreted xylanase expression per mL of culture filtrate

Fig. 5 Biochemical characterization of the four xylanases. **a** Effect of temperature on xylanase activity. **b** Effect of preincubation for 1 h at the indicated temperatures. **c** Effect of pH on activity. **d** Relative activity of each xylanase on various substrates, where the substrate giving the highest specific activity was 100 %. Birchwood xylan, beechwood xylan, wheat arabinoxylan, arabinan, carboxymethyl cellulose 4 M, glucomannan, and xyloglucan are indicated as birch, beech, wheat, arab, CMC, GM, and XG, respectively. Each assay was done in triplicate and the vertical bars indicate the standard deviations



preincubation at 80 °C (Fig. 5b). In contrast, *OpXyn11A* and *CcXyn11C* lost significant activity during preincubations at 40 and 60 °C, respectively. The pH optimum of *GtXyn10A* was 3.4, *GtXyn10B* was 4.5, *OpXyn11A* was 4.5, and *CcXyn11C* was 6.5 (Fig. 5c). Following 24 h preincubations at 4 °C in solutions ranging from pH 3 to 8, all four xylanases retained full activity (data not shown). Substrate specificity assays (Fig. 5d) revealed that the four xylanases exhibited 2.5- to 10-fold higher levels of activity on the xylan substrates than they exhibited on arabinan or CMC-4 M. *GtXyn10A* and *OpXyn11A* exhibited activity on xyloglucan that was equivalent to that on arabinan, while the other two xylanases did not exhibit detectable activity on xyloglucan. *OpXyn11A* was the only xylanase to display significant activity on glucomannan. *OpXyn11A* exhibited very similar activity on both arabinan and xyloglucan.

Analysis of the products of xylan hydrolysis

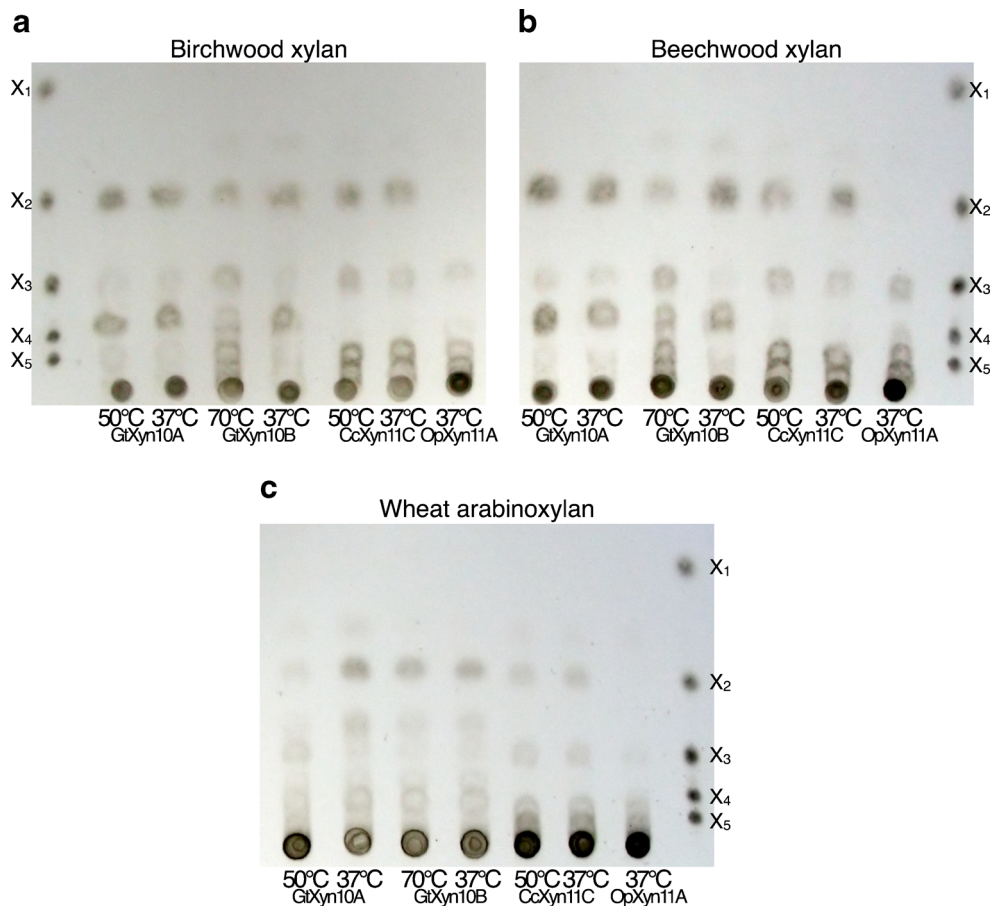
TLC and mass spectrometry were used to examine the hydrolysis products generated with three types of xylan substrates (Figs. 6 and 7 and Table 3). The hydrolysis products produced by a given xylanase using both birchwood and beechwood xylan substrates were very similar. In contrast, the product profiles produced by each xylanase were different when using hardwood versus wheat xylan. The

family 10 xylanases produced essentially identical product profiles when using the same substrate, whereas the product profiles produced by the two GH11 xylanases differed from one another and from the profiles produced by the two GH10 xylanases.

TLC analysis revealed that the major unsubstituted products generated by *GtXyn10A*, *GtXyn10B*, and *CcXyn11C*—using all four substrates—were xylobiose (X_2) and xylotriose (X_3), whereas *OpXyn11A* produced X_3 without producing significant amounts of X_2 . The TLC results also identified products with Rf values between those of the unsubstituted oligomers used as standards, suggesting the presence of products with side chains (Fig. 6). The shortest substituted product produced by the GH10 xylanases using wheat arabinoxylan was apparently X_2 with a side chain, whereas the shortest branched product they produced using birchwood or beechwood xylan was X_3 with a side chain. In contrast, the shortest substituted hydrolysis product detected following hydrolysis with the GH11 xylanases was X_4 with a side chain regardless of the xylan (Fig. 6).

The data obtained by mass spectrometry complemented the TLC results and helped to confirm the identity of hydrolysis products with [Me]GlcA substituents. MALDI-TOF analysis of the products of hardwood xylan hydrolysis by the GH10 xylanases identified relatively large peaks of X_3 , [Me]GlcA- X_3 , [Me]GlcA- X_4 , ([Me]GlcA) $_2$ - X_5 , and ([Me]GlcA) $_2$ - X_6 ,

Fig. 6 TLC analysis of 24-h reaction products. Products released after 24 h of incubation of xylanases *GtXyn10A*, *GtXyn10B*, *CcXyn11C*, and *OpXyn11A* with xylan substrates, **a** birchwood xylan, **b** beechwood xylan, and **c** wheat arabinoxylan. For **a**, **b**, two lanes are shown for *GtXyn10A*, *GtXyn10B*, and *CcXyn11C* on each plate: one for reactions at 37 °C and the second for reactions at the temperature optimum for each enzyme. Only one lane is shown for *OpXyn11A* because its temperature optimum is close to 37 °C. The standards used are xylose (X_1), xylobiose (X_2), xylotriose (X_3), xylotetraose (X_4), and xylopentaose (X_5)



and much smaller peaks of X_4 , [Me]GlcA- X_5 , [Me]GlcA- X_6 , ($[\text{Me}]$ GlcA)₂- X_7 , and ($[\text{Me}]$ GlcA)₂- X_8 . Noteworthy were the very minor peaks or absence of peaks representing unsubstituted xylo-oligomers longer than X_4 and singly substituted X_7 and X_8 (Fig. 7 and Table 3).

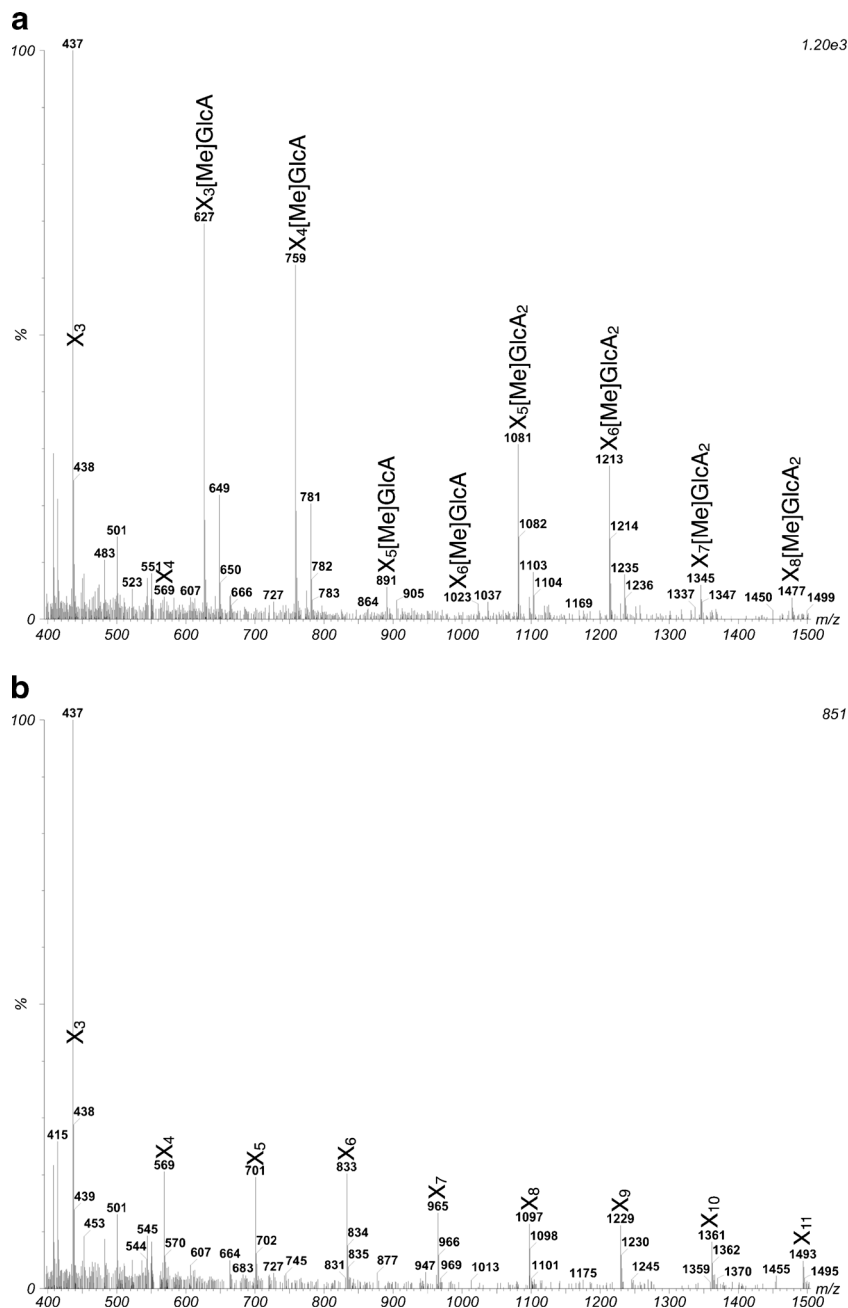
Mass spectrometry of the hardwood xylan hydrolysates obtained with the GH11 xylanases (Table 3) identified X_3 as the major unsubstituted peak, [Me]GlcA- X_4 as a minor but clearly discernible peak, and larger peaks of [Me]GlcA- X_5 , [Me]Glc- X_6 , and [Me]Glc- X_7 . Minor peaks of singly and multiply substituted longer xylo-oligosaccharides were also detected. The hardwood hydrolysate profiles obtained with the two GH11 xylanases differed in that the *OpXyn11A* profile included minor peaks of X_5 and X_6 that were not present in the *CcXyn11C* profile. Furthermore, hardwood hydrolysis with both GH11 xylanases produced profiles that included minor but detectable peaks of [Me]Glc- X_7 and [Me]Glc- X_8 , which were not observed with the GH10 xylanases.

Since arabinose and xylose are stereoisomers, digests of wheat arabinoxylan with the GH10 and GH11 xylanases produced peaks within the selected mass range, labeled X_3 through X_{11} , that have masses consistent with either xylo- or

arabino-xylo-oligosaccharides. Nonetheless, because only very minor peaks for unsubstituted xylo-oligomers of X_4 or longer were detected when hardwood xylan was the substrate, the peaks indicated X_5 through X_{11} almost certainly represent xylo-oligosaccharides substituted with at least one arabinose residue (Fig. 7 and Table 3).

TLC analysis of the products produced by the hydrolysis of xylo-oligosaccharides by the two GH10 xylanases and *CcXyn11C* revealed similar product profiles; however, a very different TLC profile was obtained with the *OpXyn11A* hydrolysate (Fig. 8). As expected, based on the TLC analysis of hydrolysis products obtained with xylans as the substrate (Fig. 6), X_2 was unchanged following treatment with the four xylanases. When X_3 , X_4 , and X_5 were the substrates, *GtXyn10A*, *GtXyn10B*, and *CcXyn11C* produced X_2 and X_3 as the major products. *GtXyn10A*, *GtXyn10B*, and *CcXyn11C* also showed transglycosylation (polymerization) activity. For example, they produced X_2 without producing detectable amounts of X_1 when X_3 was the substrate. In contrast, *OpXyn11A* was unable to hydrolyze X_3 and X_4 , and when X_5 was the substrate, it produced X_3 , X_4 , and products longer than X_5 , but did not produce detectable amounts of X_2 . The inability of *OpXyn11A* to produce X_2 when using X_5 as

Fig. 7 Sample of MALDI spectra of digestion products by *GtXyn10A*. **a** Birchwood xylan and **b** wheat arabinoxylan. X xylose residue, $[Me]GlcA$ methylated glucuronic acid residue. The masses in Daltons of selected peaks are indicated in the body of the figure. Complete set of MALDI data obtained from all four xylanases has been summarized in Table 3



the substrate (Fig. 8) is similar to the results we obtained with the various xylans as substrate, where *OpXyn11A* failed to produce significant amounts of X_2 (Fig. 6).

Discussion

Four fungal xylanases were cloned, expressed, and characterized. The four xylanases cover a broad spectrum of pH (from pH 3.4 to 6.5) and temperature (40–70 °C) optima. The *OpXyn11A* and *GtXyn10A* xylanases exhibit temperature

and pH optima that overlap the conditions used for the growth of several xylose fermenting yeasts, *Pichia stipitis*, *Candida shehatea*, and *Pachysolen tannophilus* (Agbogbo and Coward-Kelly 2008; du Preez et al. 1986; Roebuck et al. 1995). These two enzymes may therefore be attractive candidates for developing xylose fermenting yeast strains for the production of second-generation biofuels.

In the detergent, starch liquefaction, pulp and paper, food and animal feed industries, acid-tolerant thermostable enzymes are in demand (Polizeli et al. 2005). *GtXyn10A*, with its high temperature optimum of 50 °C and low pH optimum

Table 3 Summary of mass spectrometry data

Product	Mass (Da)	<i>GtXyn10A/B</i>		<i>OpXyn11A</i>		<i>CcXyn11C</i>	
		Birch ^a	Wheat ^b	Birch ^a	Wheat ^b	Birch ^a	Wheat ^b
X ₃	438	✓	✓	✓	✓	✓	✓
X ₄	569	✓	✓	✓	✓	✓	✓
X ₃ [Me]GlcA	627	✓					
X ₅	701		✓	✓	✓		✓
X ₄ [Me]GlcA	759	✓		✓		✓	
X ₆	833		✓	✓	✓		✓
X ₅ [Me]GlcA	891	✓		✓		✓	
X ₇	965		✓		✓		✓
X ₆ [Me]GlcA	1,023	✓		✓		✓	
X ₅ [Me]GlcA ₂	1,081	✓					
X ₈	1,097		✓		✓		✓
X ₇ [Me]GlcA	1,155			✓		✓	
X ₆ [Me]GlcA ₂	1,213	✓				✓	
X ₉	1,229		✓		✓		✓
X ₈ [Me]GlcA	1,287			✓		✓	
X ₇ [Me]GlcA ₂	1,345	✓		✓		✓	
X ₁₀	1,361		✓		✓		✓
X ₉ [Me]GlcA	1,419			✓			
X ₈ [Me]GlcA ₂	1,477	✓		✓		✓	
X ₁₁	1,493		✓		✓		✓

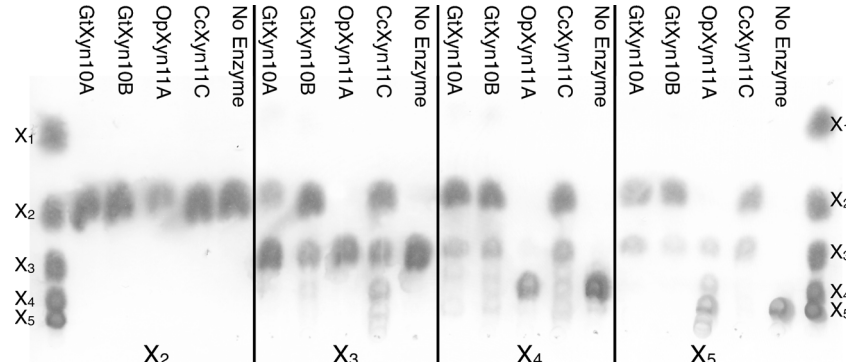
Hydrolysis products from
^a birchwood xylan and ^b wheat
arabinoxylan. *X* xylose residue,
 $[Me]GlcA$ methylated glucuronic
acid residue, ✓ masses detected
by MALDI-TOF MS

of 3.5, may be of particular interest for applications in these areas given the rarity of xylanases possessing these characteristics, since as of April 2013, only three of 243 xylanases with pH and temperature optima determined had a pH optimum ≤ 3.5 and a temperature optimum ≥ 50 °C (BRENDA, <http://www.brenda-enzymes.info/>).

Family 10 xylanases have been reported to possess subsites adjacent to the active site that bind arabinose side chains substituents attached to the -2 xylose residue (Vardakou et al. 2005) or 4-*O*-methyl-D-glucuronic acid side chains attached to the +1, +3, +4, or -3 xylose residues (Pell et al. 2004). The TLC results suggest that the two GH10 xylanases

cleave the xylan backbone more efficiently near xylose residues substituted with arabinose side chains rather than near residues with [Me]GlcA acid side groups, since the smallest substituted products detected by TLC were X_2 with an arabinose side chain and X_3 with a [Me]GlcA side chain. The 3D models of the xylanases with arabino-xylo-oligomers bound support these possibilities (Fig. 4). Note that the arabinose residue, shown in black, is difficult to distinguish from the xylose residues. It seems likely, therefore, that with an X_3 -[Me]GlcA, the third xylose residue would sit in place of the arabinose residue depicted in Fig. 4, where the bulkier [Me]GlcA side chain is unlikely to fit.

Fig. 8 TLC analysis of the products of oligosaccharide digestion. Products of 24-h reactions using the substrates xylobiose (X_2), xylotriose (X_3), xylotetraose (X_4), and xylopentaose (X_5). The standards used are xylose (X_1), X_2 , X_3 , X_4 , and X_5 .



GtXyn10A, *GtXyn10B*, and *CcXyn11C* showed very similar activities when xylose oligomers were used as the substrates. All three enzymes were inactive on xylobiose and active on xylotriose, xylotetraose, and xylopentaose. Using the three longer oligomers, they produced xylobiose and xylotriose as the major products and showed significant transglycosylation activity with xylotriose and xylotetraose. The behavior of *OpXyn11A* differed significantly from the other xylanases. *OpXyn11A* only showed significant activity with xylopentaose, and, unlike the other xylanases, it did not generate xylobiose as a product of xylopentaose hydrolysis. *OpXyn11A* did, however, produce xylotriose and showed significant transglycosylation activity.

We can see from the GH11 models that the substrate-binding cleft is only as long as five xylose residues. We therefore suggest that the single amino acid difference, Asn48 versus Ser52, between *EnXyn11A* and *OpXyn11A* reduces substrate affinity adjacent to the catalytic residues such that substrate binding to all available subsites is required for activity. In the case of *EnXyn11A*, this residue apparently facilitates xylo-oligomer binding, and therefore hydrolysis. A recent review included an alignment of 164 GH11 xylanases (Paës et al. 2012). The majority of these, 76.2 %, had an asparagine at this position, with the second most common residue being an aspartate at 19.5 %. Only five, all bacteria from the *Ruminococcus* genus, had a serine at this position, therefore *OpXyn11A* is the only eukaryotic xylanase with a serine at this position. Since *OpXyn11A* seems incapable of cleaving X₅ without prior transglycosylation into X₁₀, it apparently includes subsites distal to those identified by Vardakou et al. (2008) that enable xylo-oligomer binding and cleavage in the absence of an asparagine or aspartate residue at the +1 subsite. Furthermore, *OpXyn11A* hydrolyzes glucomannan, arabinan, and xyloglucan, which contrasts most GH11 xylanases whose substrate specificities are highly homogeneous (Paës et al. 2012). Based on these observations, we suggest that in the absence of transglycosylation, an asparagine or aspartate residue at the +1 subsite is important for the binding and hydrolysis of xylo-oligosaccharides that are five or four residues in length. We also suggest that an asparagine or aspartate residue at the +1 subsite is an important determinant of the high substrate specificity observed for the vast majority of GH11 xylanases (Paës et al. 2012).

We are in the process of generating crystal structures of the two GH11s for further comparison and also plan to generate mutants of *OpXyn11A* and *CcXyn11C*, in order to assess how the presence of a serine versus asparagine or aspartate at the +1 subsite affects substrate selectivity.

Acknowledgments This work was supported by a Collaborative Research and Development Grant (CRDPJ 385439–09) and a Strategic Network Grant (NETGP 350246–07) from the Natural Sciences and Engineering Research Council of Canada (NSERC) to Reginald Storms and Justin Powłowski.

References

- Agbogbo FK, Coward-Kelly G (2008) Cellulosic ethanol production using the naturally occurring xylose-fermenting yeast, *Pichia stipitis*. *Biotechnol Lett* 30:1515–1524. doi:[10.1007/s12010-007-9086-7](https://doi.org/10.1007/s12010-007-9086-7)
- Arnold K, Bordoli L, Kopp J, Schwede T (2006) The SWISS-MODEL workspace: a web-based environment for protein structure homology modelling. *Bioinformatics* 22:195–201. doi:[10.1093/bioinformatics/bti770](https://doi.org/10.1093/bioinformatics/bti770)
- Atlas RM, Park LC (1993) Handbook of microbiological media for the examination of food. CRC Press Inc, London
- Bajpai P (2004) Biological bleaching of chemical pulps. *Crit Rev Biotechnol* 24:1–58. doi:[10.1080/07388550490465817](https://doi.org/10.1080/07388550490465817)
- Beg QK, Kapoor M, Mahajan L, Hoondal GS (2001) Microbial xylanases and their industrial applications: a review. *Appl Microbiol Biotechnol* 56:326–338. doi:[10.1007/s002530100704](https://doi.org/10.1007/s002530100704)
- Bendtsen JD, Nielsen H, von Heijne G, Brunak S (2004) Improved prediction of signal peptides: SignalP 3.0. *J Mol Biol* 340:783–795. doi:[10.1016/j.jmb.2004.05.028](https://doi.org/10.1016/j.jmb.2004.05.028)
- Benkert P, Tosatto SC, Schomburg D (2008) QMEAN: a comprehensive scoring function for model quality assessment. *Proteins* 71:261–277. doi:[10.1002/prot.21715](https://doi.org/10.1002/prot.21715)
- Biely P (1985) Microbial xylanolytic systems. *Trends Biotechnol* 3:286–290. doi:[10.1016/0167-7799\(85\)90004-6](https://doi.org/10.1016/0167-7799(85)90004-6)
- Bromley JR, Busse-Wicher M, Tryfona T, Mortimer JC, Zhang Z, Brown D, Dupree P (2013) GUX1 and GUX2 glucuronyltransferases decorate distinct domains of glucuronoxylan with different substitution patterns. *Plant J* 74(3):423–434. doi:[10.1111/tpj.12135](https://doi.org/10.1111/tpj.12135)
- Cantarel BL, Coutinho PM, Rancurel C, Bernard T, Lombard V, Henrissat B (2009) The Carbohydrate-Active Enzymes database (CAZy): an expert resource for glycogenomics. *Nucleic Acids Res* 37:D233–D238. doi:[10.1093/nar/gkn663](https://doi.org/10.1093/nar/gkn663)
- Collins T, Gerday C, Feller G (2005) Xylanases, xylanase families, and extremophilic xylanases. *FEMS Microbiol Rev* 29:3–23. doi:[10.1016/j.femsre.2004.06.005](https://doi.org/10.1016/j.femsre.2004.06.005)
- Courtin CM, Delcour JA (2002) Arabinoxylans and endoxylanases in wheat flour bread-making. *J Cereal Sci* 35:225–243. doi:[10.1006/jcrs.2001.0433](https://doi.org/10.1006/jcrs.2001.0433)
- Cowieson AJ, Hruby M, Pierson EE (2006) Evolving enzyme technology: impact on commercial poultry nutrition. *Nutr Res Rev* 19:90–103. doi:[10.1079/NRR2006121](https://doi.org/10.1079/NRR2006121)
- Davies G, Henrissat B (1995) Structures and mechanisms of glycosyl hydrolases. *Structure* 3:853–859. doi:[10.1016/S0969-2126\(01\)00220-9](https://doi.org/10.1016/S0969-2126(01)00220-9)
- de Castro E, Sigrist CJ, Gattiker A, Bulliard V, Langendijk-Genevaux PS, Gasteiger E, Bairoch A, Hulo N (2006) ScanProsite: detection of PROSITE signature matches and ProRule-associated functional and structural residues in proteins. *Nucleic Acids Res* 34:W362–W365. doi:[10.1093/nar/gkl124](https://doi.org/10.1093/nar/gkl124)
- Decelle B, Tsang A, Storms RK (2004) Cloning, functional expression, and characterization of three *Phanerochaete chrysosporium* endo-1, 4-β-xylanases. *Curr Genet* 46:166–175. doi:[10.1007/s00294-004-0520-x](https://doi.org/10.1007/s00294-004-0520-x)
- du Prez JC, Bosch M, Prior BA (1986) Xylose fermentation by *Candida shehatae* and *Pichia stipitis*: effects of pH, temperature, and substrate concentration. *Enzym Microb Technol* 8:360–364. doi:[10.1016/0141-0229\(86\)90136-5](https://doi.org/10.1016/0141-0229(86)90136-5)
- Gilkes NR, Henrissat B, Kilburn DG, Miller RC Jr, Warren RA (1991) Domains in microbial β-1, 4-glycanases: sequence conservation, function, and enzyme families. *Microbiol Rev* 55:303–315
- Gomez LD, Steele-King CG, McQueen-Mason SJ (2008) Sustainable liquid biofuels from biomass: the writing's on the walls. *New Phytol* 178:473–485. doi:[10.1111/j.1469-8137.2008.02422](https://doi.org/10.1111/j.1469-8137.2008.02422)
- Grabber JH, Ralph J, Lapierre C, Barriere Y (2004) Genetic and molecular basis of grass cell-wall degradability. I. Lignin-cell wall matrix interactions. *C R Biol* 327:455–465. doi:[10.1016/j.crvi.2004.02.009](https://doi.org/10.1016/j.crvi.2004.02.009)

- Granström TB, Izumori K, Leisola M (2007) A rare sugar xylitol. Part II: biotechnological production and future applications of xylitol. *Appl Microbiol Biotechnol* 74:273–276. doi:[10.1007/s00253-006-0760-4](https://doi.org/10.1007/s00253-006-0760-4)
- Grishutin SG, Gusakov AV, Markov AV, Ustinov BB, Semenova MV, Sinitsyn AP (2004) Specific xyloglucanases as a new class of polysaccharide-degrading enzymes. *Biochim Biophys Acta* 1674: 268–281. doi:[10.1016/j.bbagen.2004.07.001](https://doi.org/10.1016/j.bbagen.2004.07.001)
- Harris GW, Jenkins JA, Connerton I, Cummings N, Lo Leggio L, Scott M, Hazlewood GP, Laurie JI, Gilbert HJ, Pickersgill RW (1994) Structure of the catalytic core of the family F xylanase from *Pseudomonas fluorescens* and identification of the xylpentose-binding sites. *Structure* 2:1107–1116. doi:[10.1016/S0969-2126\(94\)00112-X](https://doi.org/10.1016/S0969-2126(94)00112-X)
- Huppert M, Walker LJ (1958) The selective and differential effects of cycloheximide on many strains of *Coccidioides immitis*. *Am J Clin Pathol* 29:291–295
- Jacobs A, Larsson PT, Dahlman O (2001) Distribution of uronic acids in xylans from various species of soft- and hardwood as determined by MALDI mass spectrometry. *Biogeosciences* 2:979–990. doi:[10.1021/bm010062x](https://doi.org/10.1021/bm010062x)
- Jänts J, Hakaniemi J, Hakulinen N, Ibatullin FM, Hoxha A, Derrick PJ, Rouvinen J, Vainiotalo P (2005) Determination of thioxyloligosaccharide binding to family 11 xylanases using electrospray ionization Fourier transform ion cyclotron resonance mass spectrometry and X-ray crystallography. *FEBS J* 272:2317–2333. doi:[10.1111/j.1742-4658.2005.04659.x](https://doi.org/10.1111/j.1742-4658.2005.04659.x)
- Juturu V, Wu JC (2012) Microbial xylanases: engineering, production, and industrial applications. *Biotechnol Adv* 30:1219–1227. doi:[10.1016/j.biotechadv.2011.11.006](https://doi.org/10.1016/j.biotechadv.2011.11.006)
- Kabel MA, van den Borne H, Vincken J, Voragen AGJ, Schols HA (2007) Structural differences of xylans affect their interaction with cellulose. *Carbohydr Polym* 69:94–105. doi:[10.1016/j.carbpol.2006.09.006](https://doi.org/10.1016/j.carbpol.2006.09.006)
- Kopp J, Schwede T (2004) The SWISS-MODEL Repository of annotated three-dimensional protein structure homology models. *Nucleic Acids Res* 32:D230–D234. doi:[10.1093/nar/gkh008](https://doi.org/10.1093/nar/gkh008)
- Kraulis J, Clore GM, Nilges M, Jones TA, Pettersson G, Knowles J, Gronenborn AM (1989) Determination of the three-dimensional solution structure of the C-terminal domain of cellobiohydrolase I from *Trichoderma reesei*. A study using nuclear magnetic resonance and hybrid distance geometry-dynamical simulated annealing. *Biochem* 28:7241–7257. doi:[10.1021/bi00444a016](https://doi.org/10.1021/bi00444a016)
- Kulkarni N, Shendye A, Rao M (1999) Molecular and biotechnological aspects of xylanases. *FEMS Microbiol Rev* 23:411–456. doi:[10.1111/j.1574-6976.1999.tb00407.x](https://doi.org/10.1111/j.1574-6976.1999.tb00407.x)
- Larkin MA, Blackshields G, Brown NP, Chenna R, McGettigan PA, McWilliam H, Valentin F, Wallace IM, Wilm A, Lopez R, Thompson JD, Gibson TJ, Higgins DG (2007) Clustal W and Clustal X version 2.0. *Bioinformatics* 23:2947–2948. doi:[10.1093/bioinformatics/btm404](https://doi.org/10.1093/bioinformatics/btm404)
- Laskowski RA, MacArthur MW, Moss DS, Thornton JM (1993) PROCHECK: a program to check the stereochemical quality of protein structures. *J Appl Crystallogr* 26:283–291. doi:[10.1107/S002188992009944](https://doi.org/10.1107/S002188992009944)
- Mandels M, Andreotti R, Roche C (1976) Measurement of saccharifying cellulase. *Biotechnol Bioeng Symp* 6:21–33
- Marchler-Bauer A, Bryant SH (2004) CD-Search: protein domain annotations on the fly. *Nucleic Acids Res* 32:W327–W331. doi:[10.1093/nar/gkh454](https://doi.org/10.1093/nar/gkh454)
- Min XJ, Butler G, Storms R, Tsang A (2005a) TargetIdentifier: a webserver for identifying full-length cDNAs from EST sequences. *Nucleic Acids Res* 33:W669–W672. doi:[10.1093/nar/gki436](https://doi.org/10.1093/nar/gki436)
- Min XJ, Butler G, Storms R, Tsang A (2005b) OrfPredictor: predicting protein-coding regions in EST-derived sequences. *Nucleic Acids Res* 33:W677–W680. doi:[10.1093/nar/gki394](https://doi.org/10.1093/nar/gki394)
- Moreau A, Roberge M, Manin C, Shareck F, Kluepfel D, Morosoli R (1994) Identification of two acidic residues involved in the catalysis of xylanase A from *Streptomyces lividans*. *Biochem J* 302(Pt 1): 291–295
- Motulsky HJ, Brown RE (2006) Detecting outliers when fitting data with nonlinear regression—a new method based on robust nonlinear regression and the false discovery rate. *BMC Bioinforma* 7:123. doi:[10.1186/1471-2105-7-123](https://doi.org/10.1186/1471-2105-7-123)
- Natesh R, Manikandan K, Bhanumoorthy P, Viswamitra MA, Ramakumar S (2003) Thermostable xylanase from *Thermoascus aurantiacus* at ultrahigh resolution (0.89 Å) at 100 K and atomic resolution (1.11 Å) at 293 K refined anisotropically to small-molecule accuracy. *Acta Crystallogr D Biol Crystallogr* 59:105–117. doi:[10.1107/S0907444902020164](https://doi.org/10.1107/S0907444902020164)
- Paës G, Berrin J-G, Beauprand J (2012) GH11 xylanases: structure/function/properties relationships and applications. *Biotechnol Adv* 30:564–592. doi:[10.1016/j.biotechadv.2011.10.003](https://doi.org/10.1016/j.biotechadv.2011.10.003)
- Pagni M, Ioannidis V, Cerutti L, Zahn-Zabal M, Jongeneel CV, Hau J, Martin O, Kuznetsov D, Falquet L (2007) MyHits: improvements to an interactive resource for analyzing protein sequences. *Nucleic Acids Res* 35:W433–W437. doi:[10.1093/nar/gkm352](https://doi.org/10.1093/nar/gkm352)
- Payan F, Leone P, Porciero S, Furniss C, Tahir T, Williamson G, Durand A, Manzanares P, Gilbert HJ, Juge N, Roussel A (2004) The dual nature of the wheat xylanase protein inhibitor XIP-I: structural basis for the inhibition of family 10 and family 11 xylanases. *J Biol Chem* 279:36029–36037
- Pell G, Taylor EJ, Gloster TM, Turkenburg JP, Fontes CM, Ferreira LM, Nagy T, Clark SJ, Davies GJ, Gilbert HJ (2004) The mechanisms by which family 10 glycoside hydrolases bind decorated substrates. *J Biol Chem* 279:9597–9605. doi:[10.1074/jbc.M312278200](https://doi.org/10.1074/jbc.M312278200)
- Peña MJ, Zhong R, Zhou GK, Richardson EA, O'Neill MA, Darvill AG, York WS, Ye ZH (2007) *Arabidopsis irregular xylem8* and *irregular xylem9*: implications for the complexity of glucuronoxylan biosynthesis. *Plant Cell* 19:549–563. doi:[10.1105/tpc.106.049320](https://doi.org/10.1105/tpc.106.049320)
- Polizeli ML, Rizzatti AC, Monti R, Terenzi HF, Jorge JA, Amorim DS (2005) Xylanases from fungi: properties and industrial applications. *Appl Microbiol Biotechnol* 67:577–591. doi:[10.1007/s00253-005-1904-7](https://doi.org/10.1007/s00253-005-1904-7)
- Quevillon E, Silventoinen V, Pillai S, Harte N, Mulder N, Apweiler R, Lopez R (2005) InterProScan: protein domains identifier. *Nucleic Acids Res* 33:W116–W120. doi:[10.1093/nar/gki442](https://doi.org/10.1093/nar/gki442)
- Reid ID, Paice MG (1994) Effect of residual lignin type and amount on biological bleaching of kraft pulp by *Trametes versicolor*. *Appl Environ Microbiol* 60:1395–1400
- Roebuck K, Brundin A, Johns M (1995) Response surface optimization of temperature and pH for the growth of *Pachysolen tannophilus*. *Enzyme Microb Technol* 17:75–78. doi:[10.1016/0141-0229\(94\)00046-T](https://doi.org/10.1016/0141-0229(94)00046-T)
- Schwede T, Kopp J, Guex N, Peitsch MC (2003) SWISS-MODEL: an automated protein homology-modeling server. *Nucleic Acids Res* 31:3381–3385. doi:[10.1093/nar/gkg520](https://doi.org/10.1093/nar/gkg520)
- Seanova N, Storms R, John T, Gaudet P, Ulycznyj P, Min XJ, Sun J, Butler G, Tsang A (2006) Generation, annotation, and analysis of an extensive *Aspergillus niger* EST collection. *BMC Microbiol* 6:7. doi:[10.1186/1471-2180-6-7](https://doi.org/10.1186/1471-2180-6-7)
- Subramaniyan S, Prema P (2002) Biotechnology of microbial xylanases: enzymology, molecular biology, and application. *Crit Rev Biotechnol* 22:33–64. doi:[10.1080/07388550290789450](https://doi.org/10.1080/07388550290789450)
- Tambor JH, Ren H, Ushinsky S, Zheng Y, Riemens A, St-Francois C, Tsang A, Powłowski J, Storms R (2012) Recombinant expression, activity screening, and functional characterization identifies three novel endo-1,4-β-glucanases that efficiently hydrolyse cellulosic

- substrates. *Appl Microbiol Biotechnol* 93(1):203–214. doi:[10.1007/s00253-011-3419-8](https://doi.org/10.1007/s00253-011-3419-8)
- van den Brink J, Selten G, van den Hombergh J (1999) Expression cloning in filamentous fungi. PCT/EP1998/008577
- Vardakou M, Flint J, Christakopoulos P, Lewis RJ, Gilbert HJ, Murray JW (2005) A family 10 *Thermoascus aurantiacus* xylanase utilizes arabinose decorations of xylan as significant substrate specificity determinants. *J Mol Biol* 352:1060–1067. doi:[10.1016/j.jmb.2005.07.051](https://doi.org/10.1016/j.jmb.2005.07.051)
- Vardakou M, Dumon C, Murray JW, Christakopoulos P, Weiner DP, Juge N, Lewis RJ, Gilbert HJ, Flint JE (2008) Understanding the structural basis for substrate and inhibitor recognition in eukaryotic GH11 xylanases. *J Mol Biol* 375:1293–1305. doi:[10.1016/j.jmb.2007.11.007](https://doi.org/10.1016/j.jmb.2007.11.007)
- Wakarchuk WW, Campbell RL, Sung WL, Davoodi J, Yaguchi M (1994) Mutational and crystallographic analyses of the active site residues of the *Bacillus circulans* xylanase. *Protein Sci* 3:467–475. doi:[10.1002/pro.5560030312](https://doi.org/10.1002/pro.5560030312)